2-D Analytical Subdomain Model of a Slotted PMSM With Shielding Cylinder

Bert Hannon[1,2], Peter Sergeant[1,2], and Luc Dupré[2]

[1]Department of Information Technology and Communications, Electrical Energy Research Group, Ghent University, Gent 9000, Belgium
[2]Department of Electrical Engineering Student Association, Electrical Energy Laboratory, Ghent University, Gent 9000, Belgium

Due to their high efficiency and power density, permanent magnet synchronous machines (PMSMs) operating at high speed have recently gained a lot of attention. The development of high-speed PMSMs requires a good understanding of the physics related to the operation of such machines. Moreover, accurate modeling tools are needed when designing high-speed electrical machines. In this paper, the subdomain modeling technique is used to analytically compute the magnetic field of an electrical machine. The idea behind this technique is to divide the machine in a number of subdomains, in which the problem is simplified. The solutions in the different subdomains are then linked by imposing physical boundary conditions. The described model immediately considers the slotting effect and the eddy-current reaction field of a shielding cylinder (SC). The SC is a conductive sleeve, which is wrapped around the magnets. Its goal is to reduce the rotor losses at high-speed operation. This paper starts by introducing the applied modeling technique and the studied machine. Second, the basics of the model and its development are discussed. Finally, the results are compared with results of a finite-element (FE) model. A very good agreement between the proposed model and the FE model is observed. This implies that the developed model is indeed a powerful modeling tool for high-speed PMSMs. Moreover, it provides great insight in the machine's physics as well.

Index Terms— **Analytical models, eddy-current reaction field, high-speed PMSM, permanent-magnet machines, slotting effect, subdomain model.**

I. Introduction

AN EVER-GROWING importance of energy efficiency and a demand for more flexible applications have led to a rising interest for highly efficient permanent magnet synchronous machines (PMSMs). Moreover, lately PMSMs operating at high speed have gained a lot of attention. Indeed, because of their high power density, and thus low weight, these machines offer a high flexibility. This increased interest implies a need for accurate techniques to model high-speed PMSMs and a need for better insight in the physical aspects of such machines.

A. High-Speed Electric Machines

Although the model's applicability is not restricted to high-speed machines, the development of such machines is a motivation for the development of the presented model. Therefore, a definition of high-speed machines is necessary. An important limiting factor for the rotational speed is the tangential speed at the outer radius of the rotor. This means that achieving high rotational speeds is relatively easy for smaller machines. The definition of high-speed electric machines can thus not solely depend on the rotational speed. Therefore, Binder and Schneider [1] introduced a definition based on both the nominal power (P_{nom}) and the rotational speed. They defined high-speed ac machines as electric machines with a minimal mechanical frequency (f_{min}) that satisfies

$$\log f_{\text{min}} = 4.27 - 0.257 \log P_{\text{nom}}. \quad (1)$$

Manuscript received December 3, 2013; revised January 10, 2014; accepted February 27, 2014. Date of publication March 3, 2014; date of current version July 7, 2014. Corresponding author: B. Hannon (e-mail: bert.hannon@ugent.be).

Color versions of one or more of the figures in this paper are available online at http://ieeexplore.ieee.org.

Digital Object Identifier 10.1109/TMAG.2014.2309325

B. Goal

The goal of this paper is to provide an accurate modeling tool for high-speed permanent-magnet machines that also increases the understanding of these machines. Two aspects require special attention: 1) the eddy-current reaction field and 2) the slotting effect.

1) Eddy-Current Reaction Field: Because of cooling difficulties, permanent demagnetization of the magnets is a major concern when designing high-speed PMSMs. A commonly proposed technique to reduce the rotor losses, and thereby the demagnetization risk, is the shielding cylinder (SC). The SC is a conductive sleeve, which is wrapped around the rotor. Asynchronous harmonics in the machine's magnetic field will induce eddy currents in the sleeve. At high frequencies, the amplitude of these currents is limited because of a low penetration depth. At the same time, according to Lenz's Law, the eddy currents will produce a magnetic field that counteracts their origin. This field is called the eddy-current reaction field. The asynchronous harmonics in the magnetic field will thus be mitigated by the SC. This means that, when designed correctly, the SC reduces the overall rotor losses.

Modeling the SC analytically is one of the biggest challenges in this paper because it requires spatial and time dependency of the solution. A commonly used technique is to separate the time and spatial aspect by first solving the stationary problem and then to use its solution as an input for a simplified time-dependent problem. This has been done in [2] for induced currents in the magnets and in [3] for induced currents in the stator conductors. This technique neglects the eddy-current reaction field and is, therefore, not suited to compute the field in an electrical machine equipped with an SC. The first goal of this paper is to build a model that simultaneously accounts for spatial and time dependency. This is done in [4] for a slotless machine.

2) Slotting Effect: In contrast with the machine in [4], the machine considered in this paper contains a slotted stator. Accounting for the effect of the slots is crucial because of the importance of rotor losses in high-speed machines. Indeed, the slots will introduce asynchronously rotating fields, which in turn will cause rotor losses. A second goal is thus to exactly consider the slotting effect. There are several techniques to model the slots analytically. These are discussed in detail in Section I-C.

C. Modeling Technique

Various modeling techniques, for a large number of machine topologies, have been presented in the literature. Reviews of these techniques can be found in [4]–[7].

1) Analytical Versus Numerical Methods: A first subdivision can be made between analytical models and models using numerical techniques, mostly the finite-element (FE) technique. FE models are characterized by high accuracy because of the ability to consider nonlinearity, realistic geometries, and so on. Moreover, when using commercial or free software packages, the development time of FE models is very low. However, when compared with analytical models, FE models typically provide less insight in the physical aspects of the modeled machine. Analytical models are also easier to parameterize and are characterized by a low computational time [6]–[13]. Since a good understanding of the machine's physics and a high flexibility are of key importance here, the choice for an analytical study is obvious.

2) Conformal Mapping Versus Subdomains: Modeling the slots analytically forms a challenge. The literature considers two major techniques to do so: 1) the subdomain technique [3]–[13] and 2) conformal mapping [14]–[18].

In a first step, the conformal mapping technique maps the slotted machine to a simple geometry. Second, the field of this geometry is computed. Finally, the solution is mapped back to the slotted PMSM. When the conformal transformation is performed exactly, the accuracy of this method is high. However, the solution becomes very complicated [6]. Therefore, permeance functions were proposed as a simplification of the exact conformal transformations [14]–[16]. However, [7] showed that these simplifications imply inaccuracies in the field under the slot openings and in the tangential field component. The torque and iron loss calculations are affected by these inaccuracies. Indeed, the computation of these quantities requires good knowledge of the magnetic induction.

An alternative is the subdomain technique, which divides the machine in a number of regions (subdomains). First, a differential equation for the magnetic scalar potential or the magnetic vector potential is solved separately for every subdomain. In a second step, the subdomains are linked by imposing physical boundary conditions. These boundary conditions now account for the slotting effect. This has the advantage of a direct insight in the effect of the slots. Moreover, the degree of accuracy can easily be controlled by the number of harmonics that are considered. Several authors have reported very good results when using the subdomain modeling technique [6]–[13].

Because of its high accuracy and a good insight in the slotting effect, the subdomain technique is chosen for this paper.

By choosing the analytical subdomain modeling technique to model a slotted PMSM with an SC, a powerful, fully parameterized model is combined with high insight in the machine's physics. This tool can be used in the further development of high-speed PMSMs.

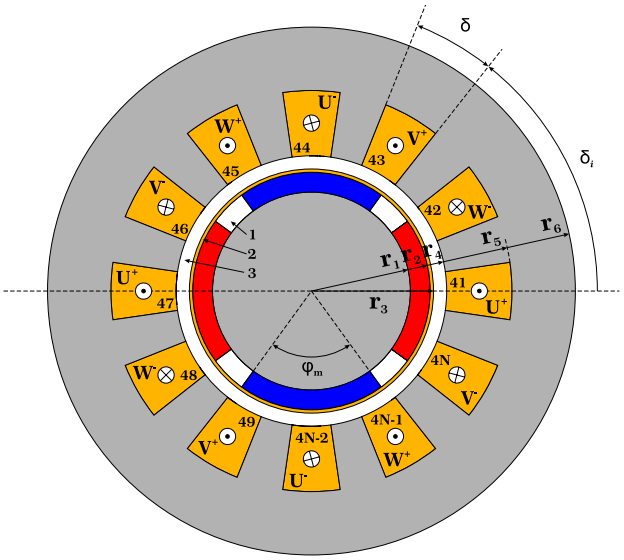

Fig. 1. Geometry of a three-phase four-pole PMSM containing an SC.

II. Geometry and Assumptions

An example of the studied machine topology is shown in Fig. 1. Note that the machine does not contain any stator teeth tips. The geometrical parameters of the machine are the rotor yoke's outer radius r_1, the magnet's outer radius r_2, the outer radius of the SC r_3, the inner radius of the stator r_4, the winding's outer radius r_5, and the machine's outer radius r_6. The magnet span is φ_m and the opening angle of the slots is δ. The angular position of the ith slot is

$$\delta_i = -\frac{\delta}{2} + \frac{2\pi}{N} i \text{ with } 1 \leq i \leq N \tag{2}$$

where N is the number of slots.

The machine is divided in a number of subdomains, as shown in Fig. 1. Every subdomain is indicated with an index ν. $\nu = 1$ stands for the PM region, 2 is the SC, and 3 is the air gap. Every slot is a separate subdomain and is indicated with an index $4i$, with i the slot number.

To enable an analytical calculation, the following assumptions are made:

1) steady-state operation;
2) infinite permeability of the rotor and stator iron;
3) relative permeability of the PM, the SC, and stator slots: $\mu_r = 1$;
4) zero conductivity of the magnets and the rotor and stator iron;
5) no induced currents in the slots;
6) radial slot boundaries;
7) no end effects.

Neglecting the influence of the induced currents on the total magnetic field is referred to as the resistance limited approximation [2], [4]. This assumption is valid if the induced currents in the SC are greater than these in the magnets.

The amplitude of the current densities at a certain depth in, respectively, the SC and the PM can be estimated as

$$J^{(2)}(r) = \frac{c}{\delta_{\mathrm{SC}}} e^{-\frac{r}{\delta_{\mathrm{SC}}}} \tag{3a}$$

$$J^{(1)}(r) = \frac{c e^{-\frac{d_{\mathrm{SC}}}{\delta_{\mathrm{SC}}}}}{\delta_{\mathrm{PM}}} e^{-\frac{r}{\delta_{\mathrm{PM}}}}. \tag{3b}$$

With c a constant, $d_{\mathrm{SC}} = r_3 - r_2$, $d_{\mathrm{PM}} = r_2 - r_1$ and δ the skin depth

$$\delta = \sqrt{\frac{2}{\omega \mu \sigma}}. \tag{4}$$

By integrating (3) over r, a measure for the induced currents in the SC and the PM (ξ) can be found. The ratio of the induced currents in the SC to the total induced currents in the rotor (R_I) can then be estimated as

$$\begin{aligned} R_I &= \frac{\xi^{(2)}}{\xi^{(1)} + \xi^{(2)}} \\ &= \frac{1 - e^{-\frac{d_{\mathrm{SC}}}{\delta_{\mathrm{SC}}}}}{e^{-\frac{d_{\mathrm{SC}}}{\delta_{\mathrm{SC}}}} \left(1 - e^{-\frac{d_{\mathrm{PM}}}{\delta_{\mathrm{PM}}}}\right) + \left(1 - e^{-e\frac{d_{\mathrm{SC}}}{\delta_{\mathrm{SC}}}}\right)}. \end{aligned} \tag{5}$$

Note that this is an underestimation. Due to electrical isolation between two magnets and a reluctance effect on higher harmonics, the actual ratio will be smaller. The authors, therefore, propose a minimum ratio of 0.6.

III. Analytical Subdomain Model

Based on Maxwell's equations and the constitutive relations, a differential equation for the magnetic vector potential in domain ν is built [4]

$$\nabla^2 \mathbf{A}^{(\nu)} - \mu_\nu \sigma_\nu \frac{\partial \mathbf{A}^{(\nu)}}{\partial t} = -\mu_\nu \mathbf{J}^{(\nu)}_{\mathbf{ext}} - \nabla \times \mathbf{B}^{(\nu)}_{\mathbf{rem}} \tag{6}$$

where $\mathbf{J}^{(\nu)}_{\mathbf{ext}}$ is an externally imposed current density, $\mathbf{B}^{(\nu)}_{\mathbf{rem}}$ stands for the remanent flux density, μ_ν is the permeability, and σ_ν is the conductivity.

The vector potential in domain ν is defined by

$$\mathbf{B}^{(\nu)} = \nabla \times \mathbf{A}^{(\nu)}. \tag{7}$$

At the boundary between two subdomains, conservation of the magnetic flux and Ampère's law are imposed. Conservation of the magnetic flux implies continuity of the vector potential. A first boundary condition can thus be written as

$$\mathbf{A}^{(\nu)} = \mathbf{A}^{(\nu+1)}. \tag{8}$$

Ampère's law implies that the tangential component of the magnetic field at one side of the boundary equals the field's tangential component at the other side plus the current density on the boundary

$$\hat{\mathbf{n}} \times \left(\mathbf{H}^{(\nu)} - \mathbf{H}^{(\nu+1)}\right) = \mathbf{K}^{(\nu)} \tag{9}$$

where $\hat{\mathbf{n}}$ is the unit vector along the normal direction and $\mathbf{K}^{(\nu)}$ is the current density on the boundary. In a 2-D model, $\mathbf{K}^{(\nu)}$ is a line current density. This paper does not consider line currents; $\mathbf{K}^{(\nu)}$ will thus always be zero.

In the following, the cylindrical coordinate system, with the z-axis along the machine's axis, is used. By neglecting the end effects, the problem can be regarded in a plane perpendicular to the z-axis. Indeed, the vector potential will only have a z-component and will only depend on the radius and the azimuth. Notice that a distinction is made between the system fixed to the stator (r, ϕ, z) and the system fixed to the rotor (r, φ, z). If θ_0 is the initial rotor position, then the stator angular position can be expressed as

$$\phi = \varphi + \Omega t + \theta_0 \tag{10}$$

where Ω is the mechanical speed of the machine.

Accounting for the induced currents in the rotor requires a clear distinction between harmonic fields that vary in time with respect to the rotor and harmonic fields that do not. Therefore, the vector potential is expressed as a function of the rotor coordinate system. However, to avoid relative movement of the boundaries between the air gap and the slots, the problem is regarded from the stator point of view. This implies the usage of $\varphi + \Omega t + \theta_0$ instead of φ.

The vector potential in the νth region can, therefore, be written as

$$\mathbf{A}^{(\nu)} = A^{(\nu)}(r, \varphi, t) \cdot \mathbf{e}_z. \tag{11}$$

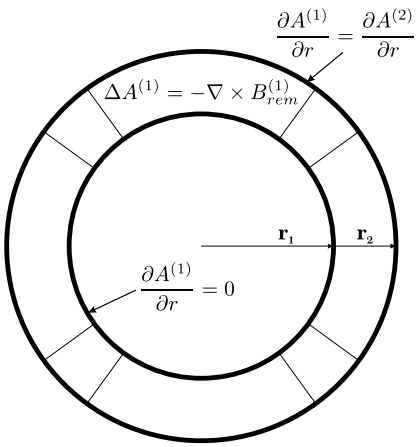

Fig. 2. PM subdomain and its boundary conditions.

IV. Magnetic Field Computation

In the following section, an expression for the vector potential will be developed based on the formal solution of (6). This is done individually for every subdomain and by making use of the separation of variables technique. The following notations will be used:

$$L_x(y, z) = \left(\frac{y}{z}\right)^x + \left(\frac{y}{z}\right)^{-x} \tag{12a}$$

$$M_x(y, z) = \left(\frac{y}{z}\right)^x - \left(\frac{y}{z}\right)^{-x} \tag{12b}$$

$$\begin{aligned} N_{w,x}(y, z) = {} & \mathrm{I}_w(\tau_{w,x} y)\, \mathrm{K}_w(\tau_{w,x} z) \\ & - \mathrm{K}_w(\tau_{w,x} y)\, \mathrm{I}_w(\tau_{w,x} z) \end{aligned} \tag{12c}$$

where I_w and K_w are the modified Bessel functions of the first and second kind and wth order, and $\tau^2_{w,x} = j(w - x)\Omega \mu_0 \sigma_2$.

A. Permanent-Magnet Subdomain

Subdomain 1 contains both the permanent magnets and the gaps between two subsequent magnets (Fig. 2). The governing

equation (6) is reduced to

$$\frac{\partial^2 A^{(1)}}{\partial r^2} + \frac{1}{r}\frac{\partial A^{(1)}}{\partial r} + \frac{1}{r^2}\frac{\partial^2 A^{(1)}}{\partial \varphi^2} = -\frac{B_{\text{rem},\varphi}}{r} - \frac{\partial B_{\text{rem},\varphi}}{\partial r} + \frac{1}{r}\frac{\partial B_{\text{rem},r}}{\partial \varphi}. \quad (13)$$

The remanent magnetic flux density, of which $B_{\text{rem},r}$ and $B_{\text{rem},\phi}$ are the radial and azimuthal components, can be written as an exponential Fourier series over space and time as

$$B_{\text{rem}}(r,\varphi,t) = \sum_{n=-\infty}^{\infty}\sum_{k=-\infty}^{\infty} B_{\text{rem},k,n}(r) e^{j(k\varphi+(k-n)\Omega t+k\theta_0)} \quad (14)$$

where n and k are the time and spatial harmonic orders, respectively. Note that the remanent magnetic induction does not vary over time when referred to the rotor coordinate system, this implies that $B_{\text{rem},k,n}(r)$ will only differ from zero if $k = n$.

At the boundary between the PM subdomain and the rotor yoke, infinite permeability of the rotor iron implies that the tangential component of the magnetic field has to be zero

$$\left.\frac{\partial A^{(1)}(r,\varphi,t)}{\partial r}\right|_{r=r_1} - \frac{B_{\text{rem},\varphi}}{\mu_0} = 0. \quad (15)$$

At $r = r_2$, continuity of the tangential component of the magnetic field condition is written as

$$\left.\frac{\partial A^{(1)}(r,\varphi,t)}{\partial r}\right|_{r=r_2} - \frac{B_{\text{rem},\varphi}}{\mu_0} = \left.\frac{\partial A^{(2)}(r,\varphi,t)}{\partial r}\right|_{r=r_2}. \quad (16)$$

When considering (15) and (16), the solution of (13) can be written as

$$A^{(1)}(r,\varphi,t) = \sum_{n=-\infty}^{\infty}\sum_{k=-\infty}^{\infty} A^{(1)}_{k,n}(r) e^{j(k\varphi+(k-n)\Omega t+k\theta_0)} \quad (17)$$

where

$$A^{(1)}_{k,n}(r) = \begin{cases} U^{(1)}_{0,n} + K_{0,n} & \text{if } k = 0 \\ \dfrac{r_2}{|k|} U^{(1)}_{k,n} \dfrac{L_{|k|}(r,r_1)}{M_{|k|}(r_2,r_1)} + K_{k,n} & \text{else.} \end{cases} \quad (18)$$

$K_{k,n}$ is the source term and depends on the magnetization of the magnets. The source term is calculated as the particular solution of (13). $K_{k,n}$ is given for radially magnetized magnets in Section VI.

The boundary condition constants $U^{(1)}_{k,n}$ are computed using the definition of an exponential Fourier constant

$$U^{(1)}_{k,n} = \frac{\Omega}{4\pi^2}\int_0^{\frac{2\pi}{\Omega}}\int_{-\Omega t-\theta_0}^{2\pi-\Omega t-\theta_0} \left.\frac{\partial A^{(2)}(r,\varphi,t)}{\partial r}\right|_{r=r_2} \cdot e^{-j(k\varphi+(k-n)\Omega t+k\theta_0)}\, \mathrm{d}\varphi \mathrm{d}t. \quad (19)$$

The spatial integration boundaries (0 and 2π) are fixed to the stator coordinate system, they are converted to the rotor coordinate system in (19). An integration over time and space has to be performed to compute the integration constants $U^{(1)}_{k,n}$. This integration is developed in the Appendix.

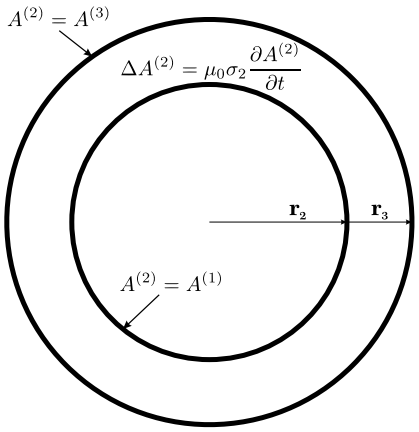

Fig. 3. SC subdomain and its boundary conditions.

B. Shielding-Cylinder Subdomain

The shielding-cylinder subdomain, as shown in Fig. 3, is the domain wherein eddy currents are induced. Its governing equation is written as

$$\frac{\partial^2 A^{(2)}}{\partial r^2} + \frac{1}{r}\frac{\partial A^{(2)}}{\partial r} + \frac{1}{r^2}\frac{\partial^2 A^{(2)}}{\partial \varphi^2} = \mu_0\sigma_2\frac{\partial A^{(2)}}{\partial t}. \quad (20)$$

It is assumed that the solution is of the same form as in the PM subdomain. This implies that, for every combination of time and spatial harmonics, the vector potential expression can be written as

$$A^{(2)}_{k,n}(r,\varphi,t) = A^{(2)}_{k,n}(r) e^{j(k\varphi+(k-n)\Omega t+k\theta_0)}. \quad (21)$$

For every individual time and spatial harmonic combination, the right-hand side of (20) can now be rewritten as

$$\mu_0\sigma_2\frac{\partial A^{(2)}_{k,n}(r,\varphi,t)}{\partial t} = j(k-n)\Omega\mu_0\sigma_2 A^{(2)}_{k,n}(r,\varphi,t) = \tau^2_{k,n} A^{(2)}_{k,n}(r,\varphi,t). \quad (22)$$

The governing equation is then rewritten as

$$\frac{\partial^2 A^{(2)}_{k,n}}{\partial r^2} + \frac{1}{r}\frac{\partial A^{(2)}_{k,n}}{\partial r} + \frac{1}{r^2}\frac{\partial^2 A^{(2)}_{k,n}}{\partial \varphi^2} = \tau^2_{k,n} A^{(2)}_{k,n}. \quad (23)$$

Both at the boundary with the magnets and at the boundary with the air gap, continuity of the vector potential has to be imposed

$$A^{(2)}(r_2,\varphi,t) = A^{(1)}(r_2,\varphi,t) \quad (24)$$

$$A^{(2)}(r_3,\varphi,t) = A^{(3)}(r_3,\varphi,t). \quad (25)$$

Accounting for the above-mentioned boundary conditions, the vector potential in the SC can be expressed as

$$A^{(2)}(r,\varphi,t) = \sum_{n=-\infty}^{\infty}\sum_{k=-\infty}^{\infty} A^{(2)}_{k,n}(r) e^{j(k\varphi+(k-n)\Omega t+k\theta_0)} \quad (26)$$

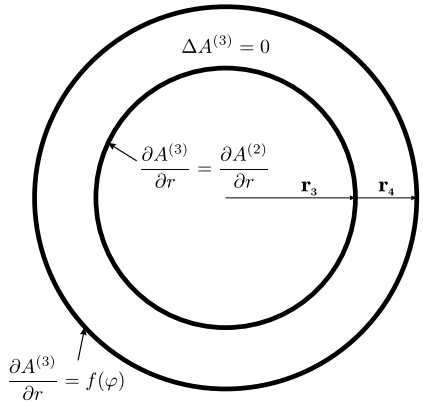

Fig. 4. Air-gap subdomain and its boundary conditions.

where

$$A_{k,n}^{(2)}(r) = \begin{cases} U_{0,0}^{(2)} \frac{\ln \frac{r}{r_3}}{\ln \frac{r_2}{r_3}} + V_{0,0}^{(2)} \frac{\ln \frac{r}{r_2}}{\ln \frac{r_3}{r_2}} & \text{if } k = n = 0 \\ U_{k,k}^{(2)} \frac{M_{|k|}(r, r_3)}{M_{|k|}(r_2, r_3)} + V_{k,k}^{(2)} \frac{M_{|k|}(r, r_2)}{M_{|k|}(r_3, r_2)} & \text{if } k = n \neq 0 \\ U_{k,n}^{(2)} \frac{N_{k,n}(r, r_3)}{N_{k,n}(r_2, r_3)} + V_{k,n}^{(2)} \frac{N_{k,n}(r, r_2)}{N_{k,n}(r_3, r_2)} & \text{else.} \end{cases} \tag{27}$$

The boundary condition constants are now written as

$$U_{k,n}^{(2)} = \frac{\Omega}{4\pi^2} \int_0^{\frac{2\pi}{\Omega}} \int_{-\Omega t - \theta_0}^{2\pi - \Omega t - \theta_0} A^{(1)}(r_2, \varphi, t) \cdot e^{-j(k\varphi + (k-n)\Omega t + k\theta_0)} \, \mathrm{d}\varphi \mathrm{d}t \tag{28a}$$

$$V_{k,n}^{(2)} = \frac{\Omega}{4\pi^2} \int_0^{\frac{2\pi}{\Omega}} \int_{-\Omega t - \theta_0}^{2\pi - \Omega t - \theta_0} A^{(3)}(r_3, \varphi, t) \cdot e^{-j(k\varphi + (k-n)\Omega t + k\theta_0)} \, \mathrm{d}\varphi \mathrm{d}t. \tag{28b}$$

The integration in (28a) and (28b) is analog as in (19).

C. Air-Gap Subdomain

In the air gap, (6) is simplified as

$$\frac{\partial^2 A^{(3)}}{\partial r^2} + \frac{1}{r} \frac{\partial A^{(3)}}{\partial r} + \frac{1}{r^2} \frac{\partial^2 A^{(3)}}{\partial \varphi^2} = 0. \tag{29}$$

The boundary condition used to rewrite the vector potential equation in the air gap is continuity of the field's tangential component. At $r = r_3$, this is (Fig. 4)

$$\left. \frac{\partial A^{(3)}(r, \varphi, t)}{\partial r} \right|_{r = r_3} = \left. \frac{\partial A^{(2)}(r, \varphi, t)}{\partial r} \right|_{r = r_3}. \tag{30}$$

At $r = r_4$, the boundary condition is written as

$$\left. \frac{\partial A^{(3)}(r, \varphi, t)}{\partial r} \right|_{r = r_4} = f(\varphi) \tag{31}$$

with

$$f(\varphi) = \begin{cases} \left. \frac{\partial A^{(4i)}(r, \varphi, t)}{\partial r} \right|_{r = r_4} & \text{if } \delta_i - \Omega t - \theta_0 \leq \varphi \leq \delta_i + \delta - \Omega t - \theta_0 \\ 0 & \text{else.} \end{cases} \tag{32}$$

Considering (30) and (31), the expression for the magnetic vector potential is formulated as

$$A^{(3)}(r, \varphi, t) = \sum_{n=-\infty}^{\infty} \sum_{k=-\infty}^{\infty} A_{k,n}^{(3)}(r) e^{j(k\varphi + (k-n)\Omega t + k\theta_0)} \tag{33}$$

where

$$A_{k,n}^{(3)}(r) = \begin{cases} A_{0,n}^{(3)} + r_3 U_{0,n}^{(3)} \ln(r) & \text{if } k = 0 \\ \frac{r_3}{|k|} U_{k,n}^{(3)} \frac{L_{|k|}(r, r_4)}{M_{|k|}(r_3, r_4)} + \frac{r_4}{|k|} V_{k,n}^{(3)} \frac{L_{|k|}(r, r_3)}{M_{|k|}(r_4, r_3)} & \text{else} \end{cases} \tag{34}$$

and $r_3 U_{0,n}^{(3)} = r_4 V_{0,n}^{(3)}$.

Note that, at every moment in time, the solution of the vector potential problem is defined except for a constant. Here, it is assumed that $A_{0,n}^{(3)} = 0$. To satisfy the boundary conditions, the integration constants are defined as

$$U_{k,n}^{(3)} = \frac{\Omega}{4\pi^2} \int_0^{\frac{2\pi}{\Omega}} \int_{-\Omega t - \theta_0}^{2\pi - \Omega t - \theta_0} \left. \frac{\partial A^{(2)}(r, \varphi, t)}{\partial r} \right|_{r = r_3} \cdot e^{-j(k\varphi + (k-n)\Omega t + k\theta_0)} \, \mathrm{d}\varphi \mathrm{d}t \tag{35a}$$

$$V_{k,n}^{(3)} = \frac{\Omega}{4\pi^2} \int_0^{\frac{2\pi}{\Omega}} \int_{-\Omega t - \theta_0}^{2\pi - \Omega t - \theta_0} f(\varphi) \cdot e^{-j(k\varphi + (k-n)\Omega t + k\theta_0)} \, \mathrm{d}\varphi \mathrm{d}t. \tag{35b}$$

The integrals in (35a) and (35b) are developed in the Appendix.

D. Slot Subdomains

A current density $\mathbf{J}_{\mathbf{ext}}^{(i)}$ is imposed in every slot i. The current flows parallel with the z-axis and is independent of r and φ. This means that the governing equation in the ith slot subdomain is

$$\frac{\partial^2 A^{(4i)}}{\partial r^2} + \frac{1}{r} \frac{\partial A^{(4i)}}{\partial r} + \frac{1}{r^2} \frac{\partial^2 A^{(4i)}}{\partial \varphi^2} = -\mu_0 J_{\mathrm{ext}}^{(i)}. \tag{36}$$

The externally imposed current density is time dependent and can be written as an exponential Fourier series

$$J_{\mathrm{ext}}^{(i)} = \sum_{n=-\infty}^{\infty} J_n^{(i)} e^{-jn\Omega t}. \tag{37}$$

Every slot has four boundaries, and the conditions on these boundaries are shown in Fig. 5 and formulated as

$$\left. \frac{\partial A^{(4i)}(r, \varphi, t)}{\partial \varphi} \right|_{\varphi = \delta_i - \Omega t - \theta_0} = 0 \tag{38}$$

$$\left. \frac{\partial A^{(4i)}(r, \varphi, t)}{\partial \varphi} \right|_{\varphi = \delta_i + \delta - \Omega t - \theta_0} = 0 \tag{39}$$

$$A^{(4i)}(r_4, \varphi, t) = A^{(3)}(r_4, \varphi, t) \tag{40}$$

$$\left. \frac{\partial A^{(4i)}(r, \varphi, t)}{\partial r} \right|_{r = r_5} = 0. \tag{41}$$

The solution of (36) can then be imposed by

$$A^{(4i)}(r, \varphi, t) = \sum_{n=-\infty}^{\infty} \sum_{l=-\infty}^{\infty} A_{l,n}^{(4i)}(r) e^{j\left(\frac{l\pi}{\delta}(\varphi - \delta_i) + \left(\frac{l\pi}{\delta} - n\right)\Omega t + \frac{l\pi}{\delta}\theta_0\right)} \tag{42}$$

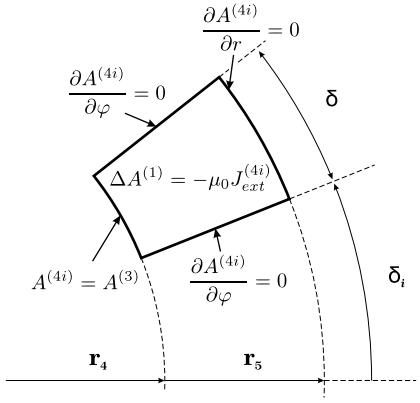

Fig. 5. ith slot subdomain and its boundary conditions.

where

$$A_{l,n}^{(4i)}(r) = \begin{cases} U_{0,n}^{(4i)} + \frac{1}{2}\mu_0 J_n^{(i)} \left(r_5^2 \ln \frac{r}{r_4} - \frac{1}{2}\left(r^2 - r_4^2\right)\right) & \text{if } l = 0 \\ U_{|l|,n}^{(4i)} \frac{L_{\left|\frac{l\pi}{\delta}\right|}(r, r_5)}{L_{\left|\frac{l\pi}{\delta}\right|}(r_4, r_5)} & \text{else.} \end{cases} \tag{43}$$

Continuity of the vector potential at $r = r_4$ is now imposed by

$$U_{|l|,n}^{(4i)} = \frac{\Omega}{4\pi^2} \int_0^{\frac{2\pi}{\Omega}} \int_{\delta_i - \Omega t - \theta_0}^{\delta_i + \delta - \Omega t - \theta_0} A^{(3)}(r_4, \varphi, t) \cdot e^{-j\left(\frac{l\pi}{\delta}(\varphi - \delta_i) + \left(\frac{l\pi}{\delta} - n\right)\Omega t + \frac{l\pi}{\delta}\theta_0\right)} \, \mathrm{d}\varphi \mathrm{d}t. \tag{44}$$

E. Conclusion

In the above sections, expressions for the vector potential in every subdomain were obtained. The integration constants in these expressions can be calculated by solving the system of boundary condition equations. Therefore, the vector potential can be calculated in every subdomain.

Note that if h_k and h_n are, respectively, the spatial and time cutoff harmonics, then the number of integration constants is $h_n(5(1 + 2h_k) + N(1 + h_k))$. This indeed complies with the number of equations, which can be calculated per boundary condition.

1) Equation (19): $h_n(1 + 2h_k)$.
2) Equation (28a): $h_n(1 + 2h_k)$.
3) Equation (28b): $h_n(1 + 2h_k)$.
4) Equation (35a): $h_n(1 + 2h_k)$.
5) Equation (35b): $h_n(1 + 2h_k)$.
6) Equation (44): $h_n N(1 + h_k)$.

The size of the resulting system is $h_n(5(1 + 2h_k) + N(1 + h_k))$. This means that the computational time will not only depend on the desired accuracy (h_k and h_n) but on the machine geometry as well (N). When very high accuracy is desired, the size of the system will be large; numerically obtaining the solution of the system will be time consuming. A study of the harmonic content of electrical machines could lead to a simplification of the system. However, the primary goal of this paper is the development of an accurate model. A further reduction of the computational time can be an interesting topic for future research.

V. Flux Density, No-Load Voltage, and Torque Computation

The magnetic vector potential can be used to compute a large number of machine characteristics. In this section, the flux density, the torque, and the no-load voltage are described.

A. Flux Density

The magnetic flux density can be computed as the curl of the vector potential (7). This means that, when a cylindrical coordinate system is used, the flux density only has a r and a φ component

$$B_r^{(\nu)} = \frac{1}{r}\frac{\partial A^{(\nu)}(r, \varphi, t)}{\partial \varphi} \text{ and } B_\varphi^{(\nu)} = -\frac{\partial A^{(\nu)}(r, \varphi, t)}{\partial r}. \tag{45}$$

B. Torque

Applying Maxwell's stress tensor in the center of the air gap ($r = r_{ac}$), the electromagnetic torque can be calculated as

$$\begin{aligned} T(t) &= \frac{l_s r_{ac}^2}{\mu_0} \int_{-\Omega t - \theta_0}^{2\pi - \Omega t - \theta_0} B_r^{(3)}(r_{ac}, \varphi, t) B_\varphi^{(3)}(r_{ac}, \varphi, t) \, \mathrm{d}\varphi \\ &= 2\pi \frac{l_s r_{ac}^2}{\mu_0} \sum_{n=-\infty}^{\infty} \sum_{s=-\infty}^{\infty} T_{n,s} e^{-j(n+s)\Omega t} \end{aligned} \tag{46}$$

where n and s represent the time harmonics of $B_r^{(4i)}$ and $B_\varphi^{(4i)}$, respectively. $T_{n,s}$ is the torque component corresponding to the time harmonic combination (n, s).

Note that the integral in (46) is analog to the integration over space in (19)

$$T_{n,s} = \sum_{k=-\infty}^{\infty} B_{r,k,n}^{(3)}(r_{ac}) B_{\varphi,-k,s}^{(3)}(r_{ac}). \tag{47}$$

The r-dependent parts of $B_{r,k,n}^{(4i)}$ and $B_{\varphi,-k,s}^{(4i)}$ can be calculated using (45).

C. No-Load Voltage

The no-load voltage induced in a phase is calculated as the time derivative of the flux coupled with that phase. If S is a surface spanned by the single turn C, then the flux coupled with that turn is calculated as

$$\lambda = \iint_S \mathbf{B} \, \mathrm{d}\mathbf{a} = \iint_S \nabla \times \mathbf{A} \, \mathrm{d}\mathbf{a} = \oint_C \mathbf{A} \, \mathrm{d}s. \tag{48}$$

Since the vector potential only has a z-component, the flux linked to a turn in slots i and $i + a$ can be calculated as

$$\lambda = l_s \left(A^{(4i)}\left(r, \delta_i + \frac{\delta}{2}, t\right) - A^{(4i+a)}\left(r, \delta_{i+a} + \frac{\delta}{2}, t\right)\right). \tag{49}$$

A matrix $\mathbf{\Lambda_{k,n}}$ can now be defined for every space and time harmonic combination as

$$\mathbf{\Lambda_{k,n}} = \begin{bmatrix} l_s A_{k,n}^{(41)}\left(r, \delta_1 + \frac{\delta}{2}\right) e^{-jn\Omega t} \\ \vdots \\ l_s A_{k,n}^{(4N)}\left(r, \delta_N + \frac{\delta}{2}\right) e^{-jn\Omega t} \end{bmatrix}. \tag{50}$$

Matrix $\mathbf{D}$ is defined as a m-by-N matrix, with m the number of phases. Every element of $\mathbf{D}$ represents the number of turns

TABLE I
PARAMETERS OF THE STUDIED MACHINE

Symbol	Parameter	Value
r_1	Rotor yoke radius	15.0 mm
r_2	Permanent magnet radius	18.0 mm
r_3	Shielding cylinder radius	18.5 mm
r_4	Air gap outer radius	20.5 mm
r_5	Slot outer radius	30.4 mm
r_6	Machine outer radius	40.0 mm
l_s	Stack length	200.0 mm
N	Number of slots	12
w	Number of windings per slot	5
δ	Slot opening angle	$0.55\frac{2\pi}{N}$ rad
B_{rem}	Remanent magnetic induction	1.2 T
p	Number of pole pairs	2
φ_m	Magnet span	$0.8\frac{\pi}{p}$ rad
I	Externally imposed current (amplitude)	50 A
f	Electrical frequency	1000 Hz
σ_2	Conductivity of the SC	$5.96 \cdot 10^7$ Ωm

a phase has in a given slot. For the single-layer winding machine, as shown in Fig. 1, $\mathbf{D}$ is

$$\mathbf{D} = \begin{bmatrix} w & 0 & 0 & -w & \cdots & 0 \\ 0 & 0 & w & 0 & \cdots & -w \\ 0 & -w & 0 & 0 & \cdots & 0 \end{bmatrix} \tag{51}$$

where w is the number of turns per winding.

If $e_j(t)$ is the no-load voltage in phase j, the no-load voltages can be computed as

$$\begin{bmatrix} e_1(t) \\ \vdots \\ e_m(t) \end{bmatrix} = \mathbf{D} \cdot \frac{\partial \boldsymbol{\Lambda}_{\boldsymbol{k,n}}}{\partial t}. \tag{52}$$

VI. VALIDATION

As validation, the machine shown in Fig. 1 will be studied using the described model. The results of this paper will be then compared with the results of an FE study. In the analytical model, the number of spatial and time harmonics has been limited to 50. The machine parameters are shown in Table I.

The magnets are radially magnetized. To simplify the source term, inverse dependency of B_{rem} on the radius is presumed. The remanent magnetic induction in the magnets can be expressed as an exponential Fourier series

$$B_{\text{rem},r}(r,\varphi,t) = \sum_{n=-\infty}^{\infty} \sum_{k=-\infty}^{\infty} B_{\text{rem},k,n}(r) e^{j(k\varphi+(k-n)\Omega t+k\theta_0)} \tag{53}$$

where

$$B_{\text{rem},k,n} = \begin{cases} j\dfrac{2r_{mc}B_{\text{rem}}\sin(k\varphi_m)}{\pi r|k|}p & \text{if } k=n \text{ and } k/p \text{ odd} \\ 0 & \text{else.} \end{cases} \tag{54}$$

The source term $K_{k,n}$ can then be calculated as

$$K_{k,n} = \begin{cases} -j\dfrac{2r_{mc}B_{\text{rem}}\sin(k\varphi_m)}{\pi k^2}p & \text{if } k=n \text{ and } k/p \text{ odd} \\ 0 & \text{else} \end{cases} \tag{55}$$

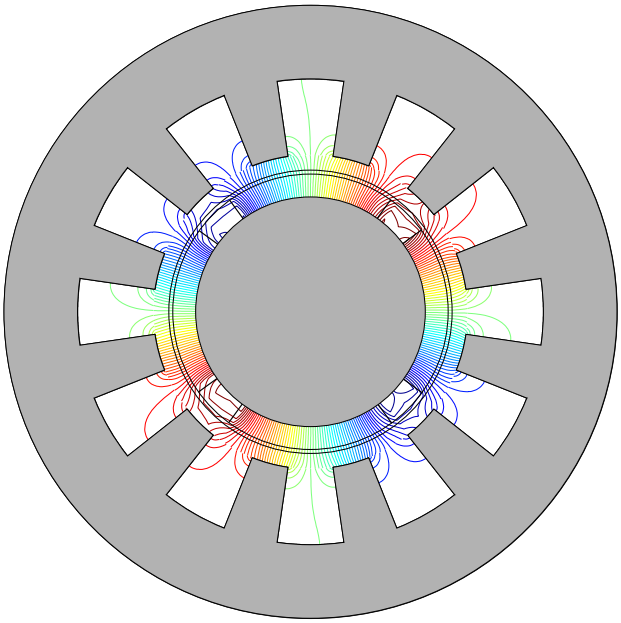

Fig. 6. Magnetic field at no-load conditions.

where r_{mc} is the radius at the center of the magnets and p is the number of pole pairs.

Although any current waveform can be applied, if its Fourier coefficients are known, in this paper, a three-phase sinusoidal system drives the machine. This means that the respective current densities in every phase can be written as

$$J_{\text{ext}}^{(i)} = \begin{cases} \dfrac{wI}{S}\dfrac{e^{-j2\Omega t}+e^{j2\Omega t}}{2} & \text{if } i \in K_U \\ \dfrac{wI}{S}\dfrac{e^{-j\left(2\Omega t-\frac{2\pi}{3}\right)}+e^{j\left(2\Omega t-\frac{2\pi}{3}\right)}}{2} & \text{if } i \in K_V \\ \dfrac{wI}{S}\dfrac{e^{-j\left(2\Omega t-\frac{4\pi}{3}\right)}+e^{j\left(2\Omega t-\frac{4\pi}{3}\right)}}{2} & \text{if } i \in K_W \end{cases} \tag{56}$$

where S is the surface of a slot and K_U, K_V, and K_W, respectively, contain the slots linked to phases U, V, and W. Note that Ω is the mechanical speed, therefore the pulsation in (56) is 2Ω.

A. No-Load Condition

When the current in the slots is set to zero, the resulting magnetic field in the discussed subdomains is shown in Fig. 6.

Notice that the boundary conditions at the boundary between the air gap and the slots are not fully satisfied. This is because of the limitation in the number of regarded harmonics.

Based on the solution of the vector potential, the magnetic induction at the center of the air gap can be calculated using (45). The results for the situation corresponding to the rotor position as in Fig. 6 are shown in Figs. 7 and 8. Note that the analytical results are in very good agreement with the results from the FE study.

The effect of the slots on the magnetic induction can be clearly observed. Fig. 9 shows the radial induction at the air gap center for different slot-opening angles.

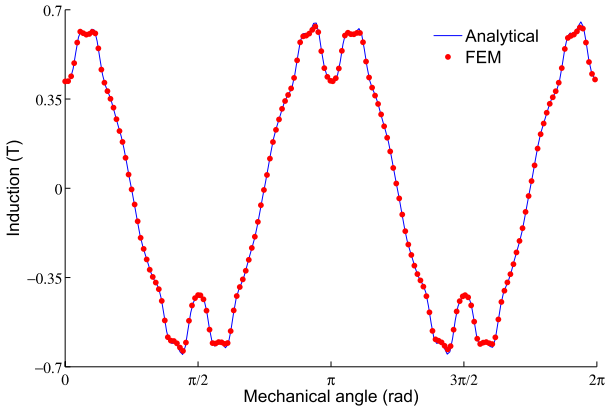

Fig. 7. Normal component of the magnetic induction in the air-gap center under no-load conditions at $t = 0$ s.

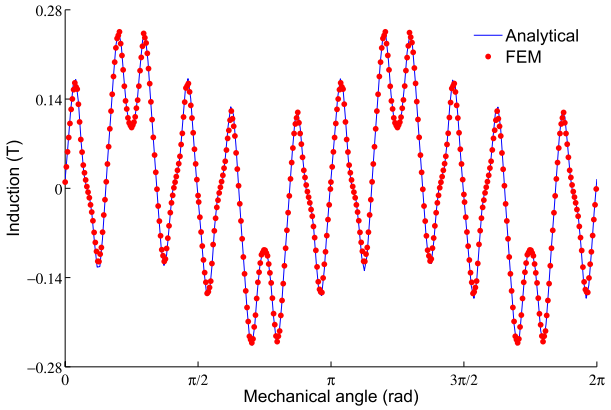

Fig. 8. Tangential component of the magnetic induction in the air-gap center under no-load conditions at $t = 0$ s.

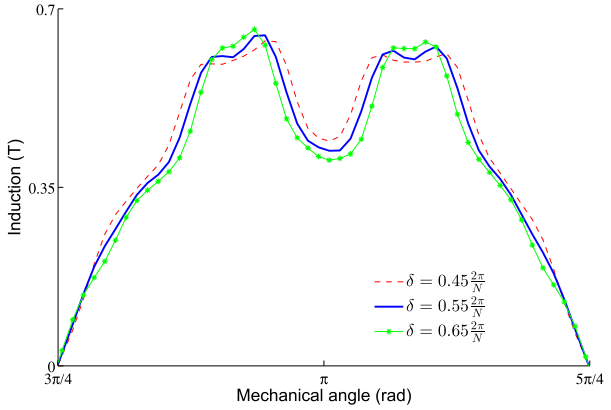

Fig. 9. Effect of the slot opening on the normal component of the magnetic induction in the air-gap center under no-load situation at $t = 0$.

At no load, the torque and no-load voltage can be computed. These results are shown in Figs. 10 and 11 when the rotor is rotated at 30 000 r/min.

The torque at no load will grow with the opening angle of the slots. A maximal difference of 4.7% between the torque obtained analytically and via FE modeling is observed. This can also be explained by a difference in permeability of the stator and rotor iron, as discussed in Section VI-C. Note that the average torque is not zero. This is because of the asynchronous magnetic fields, induced by the slotting effect. The SC acts as the squirrel cage of an induction motor, which explains the net torque.

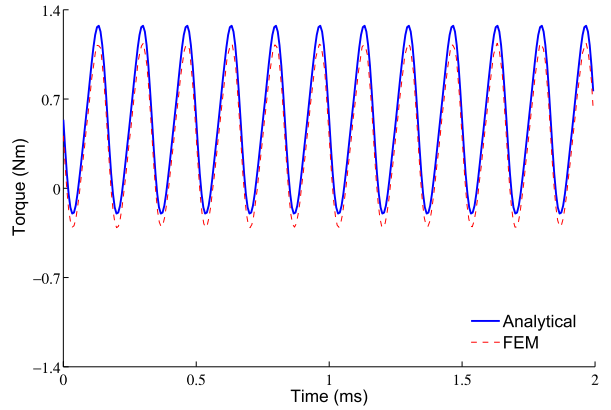

Fig. 10. Torque at no load.

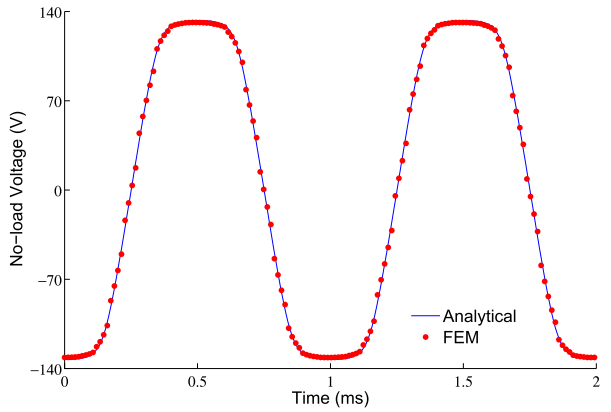

Fig. 11. No-load voltage in phase U at 30 000 r/min.

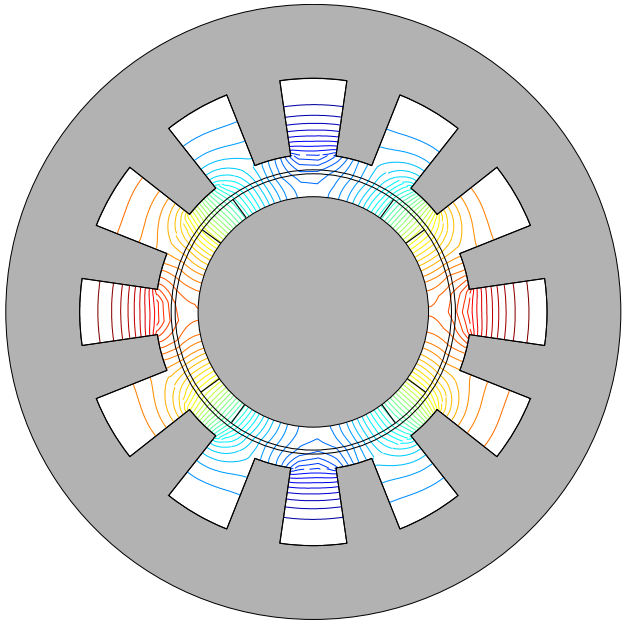

Fig. 12. Armature reaction field.

The different windings of a single phase are connected in series.

B. Armature Reaction Field

The armature reaction field is obtained when the effect of the magnets is neglected. If the rated current (50 A) is applied, the magnetic field is shown in Fig. 12.

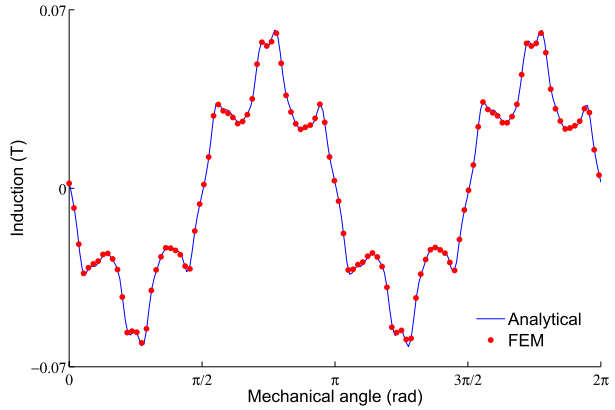

Fig. 13. Normal component of the magnetic induction in the air-gap center due to the armature reaction at $t = 0$ s.

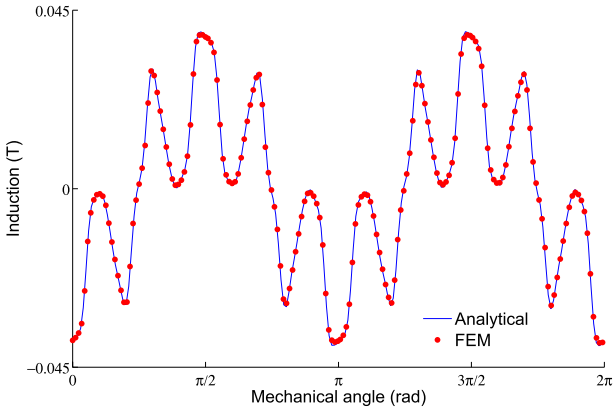

Fig. 14. Tangential component of magnetic induction in the air-gap center due to the armature reaction at $t = 0$ s.

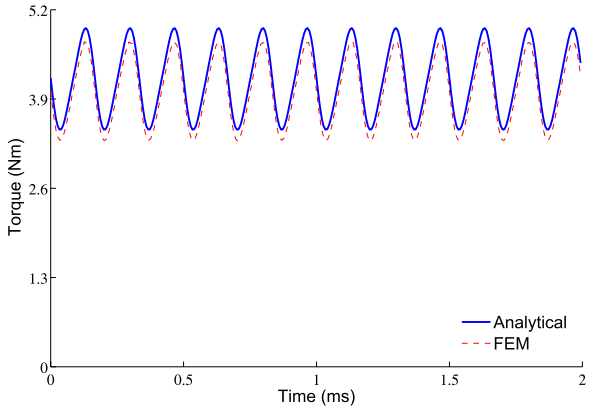

Fig. 15. Electromagnetic torque under load conditions.

The radial and tangential induction in the center of the air gap is plotted in Figs. 13 and 14. Again, very good agreement between the analytical and FE solution is obtained.

C. Load Condition

When the effects of the magnets and the stator currents are considered at the same time, the electromagnetic torque can be calculated (Fig. 15). The torque ripple has a frequency equaling N times the machine's mechanical frequency.

From Fig. 15, it can be observed that the resulting torque is smaller when using FE methods. However, the deviation is limited to 3.9%. In the analytical model, infinite permeability of the stator and rotor iron is assumed. The FE model in contrast does not account for infinite permeability. This partially explains the deviation. It is also believed that the numerical integration of the Maxwell stress tensor in the FE model causes an error.

VII. Conclusion

The above-presented validation shows that the analytical model accurately considers both the slotting effect and the SCs eddy-current reaction field. A very important feature of the model is that all the results are available separately for every space and time harmonic combination. This implies a great insight in the machine. Under no-load conditions, for example, the source term only contains harmonic combinations where the spatial harmonic order equals the time harmonic order. However, in the resulting magnetic field, other combinations are present as well. Study of these combinations gives a clear insight in the slotting effect.

When analyzing the computational time, the calculation of the boundary condition constants is dominant. However, based on these constants, all the further information, at every instance of time, can be calculated very fast.

The presented model is fast, accurate, and complete; moreover, it provides a good insight in the machine's physics. Therefore, the model meets the demands provided in Section I. It can be used to further study and optimize high-speed electrical machines.

The presented analytical model can thus be seen as a starting point for further research. The calculation of the different machine losses would be a very interesting study, certainly for high-speed machines. Other possibilities for future research are the effect of the SC on the rotor losses and a comparison with other machine types, such as the slotless PMSM or axial flux machines. Finally, one of the assumptions made in this paper is neglecting the end effects; this is only valid for sufficiently high length-to-diameter ratios. The range of validity of this assumption would be an interesting topic.

Appendix

To compute the boundary condition constants, an integration over time and space has to be done. These integrations can be developed analytically. A distinction is made between boundaries with equal spatial periods, such as the boundary between the SC and the air gap, and boundaries with different spatial periods, i.e., the boundary between the air gap and the slots. Note that the solution of the vector potential is always written in the same form

$$A^{(\nu)}(r,\varphi,t) = \sum_{n=-\infty}^{\infty} \sum_{z=-\infty}^{\infty} A_{z,n}^{(\nu)}(r) e^{j(z\varphi+(z-n)\Omega t+z\theta_0)}. \quad (57)$$

In the latter, z can either be an integer (k) or $l\pi/\delta$, where l is an integer.

At boundaries with equal spatial periods [(19), (28a), (28b) and (35a)], the integration will be of the form, as illustrated in (58)

$$\int_0^{\frac{2\pi}{\Omega}} \int_{-\Omega t-\theta_0}^{2\pi-\Omega t-\theta_0} \left(\sum_{s=-\infty}^{\infty} \sum_{q=-\infty}^{\infty} e^{j(q\varphi+(q-s)\Omega t+q\theta_0)} \right) \cdot e^{-j(k\varphi+(k-n)\Omega t+k\theta_0)} \, \mathrm{d}\varphi \mathrm{d}t. \quad (58)$$

The integration can then be developed for every time and spatial harmonic combination (q,s)

$$\int_0^{\frac{2\pi}{\Omega}} \int_{-\Omega t-\theta_0}^{2\pi-\Omega t-\theta_0} e^{j(q\varphi+(q-s)\Omega t+q\theta_0)} e^{-j(k\varphi+(k-n)\Omega t+k\theta_0)}\, \mathrm{d}\varphi \mathrm{d}t = \begin{cases} \dfrac{4\pi^2}{\Omega} & \text{if } s=n \text{ and } q=k \\ 0 & \text{else.} \end{cases} \tag{59}$$

The integration in (35b) will be written as

$$\sum_{i=1}^{N} \int_0^{\frac{2\pi}{\Omega}} \int_{\delta_i-\Omega t-\theta_0}^{\delta_i+\delta-\Omega t-\theta_0} \left(\sum_{s=-\infty}^{\infty} \sum_{q=-\infty}^{\infty} e^{j\left(\frac{q\pi}{\delta}(\varphi-\delta_i)+\left(\frac{q\pi}{\delta}-s\right)\Omega t+\frac{q\pi}{\delta}\theta_0\right)} \right) \cdot e^{-j(k\varphi+(k-n)\Omega t+k\theta_0)}\, \mathrm{d}\varphi \mathrm{d}t. \tag{60}$$

The development of (60) can be written per time and spatial harmonic combination as

$$\int_0^{\frac{2\pi}{\Omega}} \int_{\delta_i-\Omega t-\theta_0}^{\delta_i+\delta-\Omega t-\theta_0} e^{j\left(\frac{q\pi}{\delta}(\varphi-\delta_i)+\left(\frac{q\pi}{\delta}-s\right)\Omega t+\frac{q\pi}{\delta}\theta_0\right)} \cdot e^{-j(k\varphi+(k-n)\Omega t+k\theta_0)}\, \mathrm{d}\varphi \mathrm{d}t = \begin{cases} \delta\dfrac{2\pi}{\Omega} e^{-jk\delta_i} & \text{if } s=n \text{ and } q=k \\ j\delta\dfrac{2\pi}{\Omega}\dfrac{1-(-1)^q e^{-jk\delta}}{q\pi-k\delta} e^{-jk\delta_i} & \text{if } s=n \text{ and } q\neq k \\ 0 & \text{else.} \end{cases} \tag{61}$$

Finally, the integration in (44) equals

$$\int_0^{\frac{2\pi}{\Omega}} \int_{\delta_i-\Omega t-\theta_0}^{\delta_i+\delta-\Omega t-\theta_0} \left(\sum_{s=-\infty}^{\infty} \sum_{q=-\infty}^{\infty} e^{j(q\varphi+(q-s)\Omega t+q\theta_0)} \right) \cdot e^{-j\left(\frac{l\pi}{\delta}(\varphi-\delta_i)+\left(\frac{l\pi}{\delta}-n\right)\Omega t+\frac{l\pi}{\delta}\theta_0\right)}\, \mathrm{d}\varphi \mathrm{d}t. \tag{62}$$

Every time and spatial combination can be developed as

$$\int_0^{\frac{2\pi}{\Omega}} \int_{\delta_i-\Omega t-\theta_0}^{\delta_i+\delta-\Omega t-\theta_0} e^{j(q\varphi+(q-s)\Omega t+q\theta_0)} \cdot e^{-j\left(\frac{l\pi}{\delta}(\varphi-\delta_i)+\left(\frac{l\pi}{\delta}-n\right)\Omega t+\frac{l\pi}{\delta}\theta_0\right)}\, \mathrm{d}\varphi \mathrm{d}t = \begin{cases} \delta\dfrac{2\pi}{\Omega} e^{jq\delta_i} & \text{if } s=n \text{ and } q=k \\ -j\delta\dfrac{2\pi}{\Omega}\dfrac{1-(-1)^l e^{jq\delta}}{l\pi-q\delta} e^{jq\delta_i} & \text{if } s=n \text{ and } q\neq k \\ 0 & \text{else.} \end{cases} \tag{63}$$

REFERENCES

[1] A. Binder and T. Schneider, "High-speed inverter-fed ac drives," in *Proc. Int. ACEMPE*, Sep. 2007, pp. 9–16.

[2] P. Sergeant and A. Van den Bossche, "Influence of the amount of permanent magnet material in fractional-slot permanent magnet synchronous machines," *IEEE Trans. Ind. Electron.*, vol. 61, no. 9, pp. 4979–4989, Sep. 2013.

[3] P. Arumugam, T. Hamiti, and C. Gerada, "Estimation of eddy current loss in semi-closed slot vertical conductor permanent magnet synchronous machines considering eddy current reaction effect," *IEEE Trans. Magn.*, vol. 49, no. 10, pp. 5326–5335, Oct. 2013.

[4] S. R. Holm, H. Polinder, and J. A. Ferreira, "Analytical modeling of a permanent-magnet synchronous machine in a flywheel," *IEEE Trans. Magn.*, vol. 43, no. 5, pp. 1955–1967, May 2007.

[5] A. Rahideh and T. Korakianitis, "Analytical calculation of open-circuit magnetic field distribution of slotless brushless PM machines," *Int. J. Electr. Power Energy Syst.*, vol. 44, no. 1, pp. 99–114, 2013.

[6] Z. Q. Zhu, L. J. Wu, and Z. P. Xia, "An accurate subdomain model for magnetic field computation in slotted surface-mounted permanent-magnet machines," *IEEE Trans. Magn.*, vol. 46, no. 4, pp. 1100–1115, Apr. 2010.

[7] Z. J. Liu and J. T. Li, "Analytical solution of air-gap field in permanent-magnet motors taking into account the effect of pole transition over slots," *IEEE Trans. Magn.*, vol. 43, no. 10, pp. 3872–3883, Oct. 2007.

[8] M. R. Shah, H. Polinder, and S. B. Lee, "Rapid analytical optimization of eddy-current shield thickness for associated loss minimization in electrical machines," *IEEE Trans. Ind. Appl.*, vol. 42, no. 3, pp. 642–649, Jun. 2006.

[9] A. Bellara, Y. Amara, G. Barakat, and B. Dakyo, "Two-dimensional exact analytical solution of armature reaction field in slotted surface mounted pm radial flux synchronous machines," *IEEE Trans. Magn.*, vol. 45, no. 10, pp. 4534–4538, Oct. 2009.

[10] Y. Amara and G. Barakat, "Analytical modeling of magnetic field in surface mounted permanent-magnet tubular linear machines," *IEEE Trans. Magn.*, vol. 46, no. 11, pp. 3870–3882, Nov. 2010.

[11] B. L. J. Gysen, E. Ilhan, K. J. Meessen, J. J. H. Paulides, and E. A. Lomonova, "Modeling of flux switching permanent magnet machines with Fourier analysis," *IEEE Trans. Magn.*, vol. 46, no. 6, pp. 1499–1502, Jun. 2010.

[12] T. Lubin, S. Mezani, and A. Rezzoug, "Exact analytical method for magnetic field computation in the air gap of cylindrical electrical machines considering slotting effects," *IEEE Trans. Magn.*, vol. 46, no. 4, pp. 1092–1099, Apr. 2010.

[13] T. Lubin, S. Mezani, and A. Rezzoug, "2-D exact analytical model for surface-mounted permanent-magnet motors with semi-closed slots," *IEEE Trans. Magn.*, vol. 47, no. 2, pp. 479–492, Feb. 2011.

[14] Z. Q. Zhu and D. Howe, "Instantaneous magnetic field distribution in brushless permanent magnet DC motors. III. Effect of stator slotting," *IEEE Trans. Magn.*, vol. 29, no. 1, pp. 143–151, Jan. 1993.

[15] H. Vansompel, P. Sergeant, and L. Dupré, "A multilayer 2-D–2-D coupled model for eddy current calculation in the rotor of an axial-flux PM machine," *IEEE Trans. Energy Convers.*, vol. 27, no. 3, pp. 784–791, Sep. 2012.

[16] M. Markovic, M. Jufer, and D. Howe, "Reducing the cogging torque in brushless DC motors by using conformal mappings," *IEEE Trans. Magn.*, vol. 40, no. 2, pp. 451–455, Mar. 2004.

[17] K. Boughara, D. Zarko, R. Ibtiouen, O. Touhami, and A. Rezzoug, "Magnetic field analysis of inset and surface-mounted permanent-magnet synchronous motors using Schwarz–Christoffel transformation," *IEEE Trans. Magn.*, vol. 45, no. 8, pp. 3166–3178, Aug. 2009.

[18] D. Zarko, D. Ban, and T. A. Lipo, "Analytical solution for cogging torque in surface permanent-magnet motors using conformal mapping," *IEEE Trans. Magn.*, vol. 44, no. 1, pp. 52–65, Jan. 2008.